CHEMISTRY OF MATERIALS

ARTICLE

pubs.acs.org/cm

Model Compounds Based on Cyclotriphosphazene and Hexaphenylbenzene with Tethered Li^+-Solvents and Their Ion-Conducting Properties

Jörg Thielen, Wolfgang H. Meyer,* and Katharina Landfester

Max Planck Institute for Polymer Research, Ackermannweg 10, D-55128 Mainz, Germany

ABSTRACT: To improve the lithium ion conductivities of currently used electrolytes, it is critical to understand how the transport of the lithium ions within the matrix is influenced by their interactions with solvating moieties. Therefore, well-defined model compounds based on cyclotriphosphazene (CTP) and hexaphenylbenzene (HPB) cores were prepared, bearing side groups containing the structural element of ethylene carbonate, which is the common solvent for lithium salts used as electrolytes in Li-ion batteries. All model compounds were highly pure and thermally stable up to at least 250 °C, covering a broad range of glass transition temperatures from −79 °C up to +3.5 °C. The temperature-dependent ionic conductivities of the blends follow a William−Landel−Ferry (WLF) type behavior with the corresponding glass transition temperatures as reference. Though the glass transition temperatures of the blends are low, their conductivities are only in the range of typical polymer electrolytes, implying that the coordination between the cyclic carbonate functionality and the Li-ion is apparently too tight to allow for fast Li-ion dynamics.

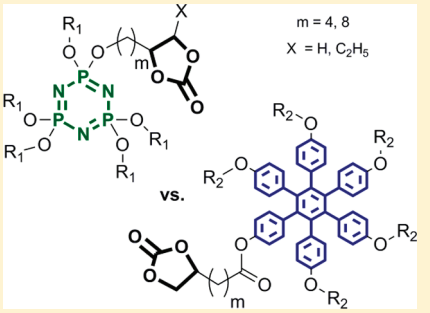

KEYWORDS: cyclotriphosphazene, hexaphenylbenzene, cyclic carbonate, lithium ion conductor, model compounds

INTRODUCTION

Efficient energy storage and conversion is playing a key role in overcoming the present and future challenges in energy supply. Batteries provide portable, electrochemical storage of green energy sources such as solar, wind, or water power, and potentially allow for a reduction of the dependence on fossil fuels, which is of great importance with respect to the issue of global warming. In view of energy density and energy drain, the development of rechargeable lithium ion batteries has to be considered as a milestone for the internal power supply of the tremendously increasing amount of mobile and portable electric and electronic devices.[1,2] In such batteries, lithium ions are solvated by an organic solvent and diffuse freely between the anode and cathode which are physically isolated by a separator membrane.[3,4] Most commonly used electrolytes comprise blends of highly polar carbonates which are reasonably good solvents for Li-salts,[5] e.g. ethylene carbonate (EC), propylene carbonate (PC), diethyl carbonate (DEC), or dimethyl carbonate (DMC).

In case of small battery packages, these electrolytes have proven to fulfill safety and market concerns in terms of high ionic conductivity at ambient temperatures (in the order of 10^{-3} S cm^{-1}) combined with a high boiling and a low melting point as well as safe performance over a wide temperature range.[6] However, the usage of organic liquids in large batteries as in electric vehicles poses potential safety hazards. Due to the high flammability and the present vapor pressure of the organic liquids, abrupt leakage when mechanical forces are applied (e.g., in car accidents) or overheating as a course of sudden and uncontrolled discharge ("short circuits") may lead to ignition or in the last resort even to explosion of the battery.[7] As a consequence, to use the electrolytes safely, technical measures such as hermetic metal encasements or relief valves are necessary, leading to a decrease in the effective energy density of the battery. Therefore, over the last decades, major efforts have been made to develop solvent-free ion conducting polymer electrolytes. Starting with Wright's discovery in 1973, showing that alkali metal salt complexes of poly(ethylene oxide) (PEO) show substantial ionic conductivity,[8] several main routes of polymer electrolytes have been developed: (i) dry solid polymer electrolytes (SPEs), (ii) gel polymer electrolytes, (iii) composite polymer electrolytes, and (iv) ionic liquids.[9−11] Despite great efforts and testing of various systems as replacements, the ideal electrolyte has not yet been identified.

Previous studies in our group based on our general approach of "immobilizing" ion solvents revealed, that tethering the structural element of EC to a poly(meth)acrylate backbone yielded rather surprising high conductivities, despite the comparably high glass transition temperatures (T_g).[12] Those did not serve as reference temperature for the conductivity in the corresponding modified William−Landel−Ferry (WLF) plot, thus suggesting that the ion mobility is controlled by side chain dipole relaxation modes rather than by the segmental motion of the polymer backbone.

Considering these results, which are indicating that the ion mobility is decoupled from the other membrane relevant properties of the polymer, model compounds were prepared to study the influence of both the glass transition temperatures and the spacer length on the ionic conductivity in more detail. Perfectly

Received: December 14, 2010
Revised: February 11, 2011
Published: March 22, 2011

defined model compounds are highly suitable for reliable analysis of the molecular ion transport, governed by the complex interplay of numerous parameters within an electrolyte, such as viscosity, salt dissociation, ion−solvent interaction, or ion association, hence affecting the bulk conductivity. It is anticipated that this study not only provides suggestions for optimization directions, but also reveals further insights into the possible ion conducting mechanism. The latter is fundamental for tailored improvement of the current electrolytes and to provide materials for low-cost secondary batteries of high voltage, capacity, and rate-capability, in strong demand for the potential mass market of electric transport and the urgent need to reduce CO_2 emissions.

In agreement with these considerations, we have chosen two series of model compounds with the objective to cover a preferably broad range of glass transition temperatures. One series is based on the relatively flexible cyclotriphosphazene (CTP). The polyphosphazene itself, which is well-known for low glass transition temperatures,[14−16] was not chosen, since building up the cyclic carbonate group from an alkenole functionalized polyphosphazene via epoxidation with 3-chloroperoxybenzoic acid potentially leads to degradation and chain cleavage due to the rather harsh and oxidative reaction conditions. Indeed, degradation and rearrangement of a variety of different functionalized polyphosphazenes is well documented,[14,16−18] but imperfectly defined substances are not suitable for the outlined investigations.

The second series is based on the rather stiff hexaphenylbenzene (HPB), possibly allowing self-assembly and local packing.[19] In both cases, the tethered cyclic carbonate (2-oxo-1,3-dioxolane) groups serve as ion solvating moieties. The spacer length between the cyclic carbonate moieties and the different cores as well as the position of the cyclic carbonate was varied, mainly to reveal the impact of the local mobility of the solvating units on the performance as lithium ion conductor.

EXPERIMENTAL SECTION

Materials. 5-hexen-1-ol, 5-cis-octen-1-ol, 9-decen-1-ol, and tetraethylene glycol monomethyl ether were dried over calcium hydride and distilled under argon before use. Tetrahydrofuran (THF, 99.9%, Acros) and dioxane (99.9%, Acros) were dried over sodium and distilled under argon before use. Acetonitrile and methylene chloride were dried with activated molecular sieves (4 Å). Hexachlorocyclotriphosphazene (99.99%, resublimed, Aldrich) and all other chemicals were used as received without further purification unless indicated otherwise. Air or moisture-sensitive reactions were performed in thoroughly flame-dried glass vessels in an inert atmosphere of dry argon using standard Schlenk techniques. Analytical thin layer chromatography (TLC) was carried out on F-254 percoated silica gel 60 plates (Machery Nagel). Visualization was performed with UV light (254 nm), potassium permanganate solution, or iodine stain. Column chromatography on all compounds was conducted with silica gel 60 (0.063−0.2 mm pore size) from Fluka.

Measurements. ^{1}H and ^{13}C NMR spectra were recorded on a Bruker AC 300 MHz and a Bruker Avance III 250 MHz spectrometer; ^{31}P NMR spectra were measured with either a Bruker Avance III 500 MHz or a Bruker Avance III 700 MHz spectrometer. ^{1}H and ^{13}C chemical shifts are quoted on the δ-scale in units of parts per million (ppm) using the residual solvent protons as internal standard. ^{31}P signal shifts were referred to triphenylphosphine (TPP) (δ = −6.00 ppm) as external reference. Coupling constants (J) are reported in hertz (Hz), and splitting patterns are designated as s (singlet), d (doublet), dd (double doublet), t (triplet), m (multiplet), and br (broad). MALDI mass spectra were obtained on a Bruker-Daltonics Reflex-Tof.

Thermogravimetric analysis (TGA) was measured under nitrogen at a heating rate of 10 K min^{-1} using a TGA/SDTA-851 (Mettler-Toledo). Differential scanning calorimetry (DSC) was carried out on a Mettler-Toledo DSC-30 under nitrogen at a heating rate of 10 K min^{-1}.

Impedance spectroscopy was recorded as a function of temperature using a Solartron SI 1260 impedance/gain phase analyzer with a high resolution dielectric converter (Alpha high-resolution dielectric analyzer, Novocontrol) in the range from 10^{-2} to 10^7 Hz. The measurements were performed using plain, polished stainless steel or platinum electrodes with a temperature controlled cryostat under N_2 (Novocontrol). Direct current (dc) conductivities were usually obtained from the lower-frequency plateau values of the real part of the alternating current (ac) conductivities (Bode plot).

Preparation of the Blends. The model compounds and the corresponding amount of the respective lithium salt were dissolved in a minimum amount of dry THF ($H_20 \leq 50$ ppm, dry DMF was used in case of **13**) in a nitrogen filled glovebox. The homogeneous solutions were concentrated in vacuum (10^{-3} mbar) at 80 °C for several days. Complete evaporation of the organic solvent was checked by NMR spectroscopy. Finally the viscous, honeylike electrolytes were placed between polished stainless steel electrodes keeping a fixed distance of the electrodes of about 0.1 mm by means of Teflon spacers.

Synthesis. *1. CTP-Based Model Compounds*

2,2,4,4,6,6-Hexakis-(5-hexenyl-1-oxy)-cyclotriphosphazene (1). 5-Hexen-1-ol (4.61 g, 46.02 mmol) was added to a suspension of NaH (95%, 1.16 g, 45.97 mmol) in 20 mL of dioxane. The mixture was stirred at 50 °C for 24 h under argon atmosphere to form the corresponding alkoxide. $N_3P_3Cl_6$ (1.32 g, 3.80 mmol) was dissolved in 60 mL freshly distilled dioxane and added dropwise to the alkoxide suspension. The resultant mixture was stirred at 60 °C for 48 h under an atmosphere of dry argon. Completion of the reaction was checked by ^{31}P NMR. The mixture was then filtrated and the solvent evaporated in vacuum. The crude product was purified by column chromatography ($CHCl_3$/MeOH, 100/1, v/v, retardation factor R_f = 0.80) leading to a colorless, viscous liquid **1** (2.13 g, 2.92 mmol, 77% yield).^{1}H NMR (DMSO, 250 MHz): δ 1.33−1.44 (m, 12H, —OCH$_2$C*H*$_2$—), 1.53−1.63 (m, 12H, —C*H*$_2$CH$_2$CH═), 1.96−2.05 (m, 12H, —C*H*$_2$—CH═), 3.77−3.85 (m, 12H, —OC*H*$_2$—), 4.91−5.04 (m, 12H, ═C*H*$_2$), 5.69−5.86 (m, 6H, —C*H*═CH$_2$).^{13}C NMR (DMSO, 250 MHz): δ 24.4, 29.1, 32.7, 64.9, 114.9, 138.4. ^{31}P NMR (DMSO, 700 MHz): δ 18.03 (s). MALDI-TOF *m*/*z* (%) 729.9 (100).

2,2,4,4,6,6-Hexakis-(4-(oxiran-2-yl)-but-1-oxy)-cyclotriphosphazene (2). 2,6-Ditert-butyl-4-methylphenol (BHT) (7.67 g, 34.81 mmol) and **1** (1.50 g, 2.06 mmol) were dissolved in 50 mL methylene chloride. The solution was cooled to 0 °C and 3-chloroperoxybenzoic acid (MCPBA) (77%, 7.81 g, 34.85 mmol) was added portionwise. The mixture was stirred vigorously for 48 h. After complete epoxidation, the mixture was washed three times with 10 wt % sodium hydroxide solution and water. The organic phase was dried over $MgSO_4$ and then concentrated to dryness. After purification by column chromatography (gradient, *n*-hexane/ethyl acetate, 5/1, v/v, passing over to ethyl acetate and finally MeOH, $R_{f,n\text{-hexane/ethylacetate},5/1}$ = 0.11) compound **2** was obtained as a slightly orange, viscous oil (1.34 g, 1.62 mmol, 79% yield). ^{1}H NMR ($CDCl_3$, 250 MHz): δ 1.35−1.80 (m, 36H, —OCH$_2$—(C*H*$_2$)$_3$—), 2.42 (dd, 6H, ^2J = 4.9, ^3J = 2.7, —CH—(—O—)—C*H*$_2$), 2.70 (dd, 6H, ^2J = 4.8, ^3J = 3.6, —CH—(—O—)—C*H*$_2$), 2.80−2.92 (m, 6H, —C*H*—(—O—)—CH$_2$), 3.80−3.95 (m, 12H, —OC*H*$_2$—). ^{13}C NMR ($CDCl_3$, 250 MHz): δ 22.5, 30.1, 32.2, 47.1, 52.3, 65.7. ^{31}P NMR (DMSO, 700 MHz): δ 17.24 (s). MALDI-TOF *m*/*z* (%) 825.9 (100).

2,2,4,4,6,6-Hexakis-(4-(4-butoxy)-1,3-dioxolan-2-one)-cyclotriphosphazene (3). Tetrabutylammonium iodide (0.18 g, 0.49 mmol), tributyltin iodide (0.20 g, 0.49 mmol), and **2** (1.34 g, 1.62 mmol) were homogenously mixed in 25 mL of THF. Under N_2 atmosphere, CO_2 was

passed continuously through the clear solution for 24 h at 50 °C. The mixture was then concentrated and the crude product was purified by column chromatography (ethyl acetate/THF, 2/1, v/v, R_f = 0.48). Product **3** was obtained as a colorless, highly viscous oil (1.01 g, 0.93 mmol, 57% yield). ^{1}H NMR (DMSO, 250 MHz): δ 1.23−1.51 (m, 12H, —OCH$_2$CH$_2$C*H*$_2$—), 1.52−1.83 (m, 24H, —OCH$_2$C*H*$_2$—, —C*H*$_2$CH—(O(C═O)O)—CH$_2$), 3.84 (m, 12H, —OC*H*$_2$—), 4.11 (dd, 6H, ^2J = 8.0, ^3J = 7.2, —CH—(O(C═O)O)—C*H*$_2$), 4.56 (dd, 6H, ^2J = 8.1, ^3J = 7.2, —CH—(O(C═O)O)—C*H*$_2$), 4.73−4.84 (m, 6H, —C*H*—(O(C═O)O)—CH$_2$). ^{13}C NMR (DMSO, 250 MHz): δ 20.5, 29.2, 32.4, 64.9, 69.2, 76.9, 154.9. ^{31}P NMR (DMSO, 500 MHz): δ 17.21 (s). MALDI-TOF *m*/*z* (%) 1090 (100).

2,2,4,4,6,6-Hexakis-(9-decenyl-1-oxy)-cyclotriphosphazene (4). Synthetic procedure followed that for compound **1** to afford **4** as colorless liquid (column chromatography, *n*-hexane/ethyl acetate, 4/1, v/v, R_f = 0.88, 82% yield). ^{1}H NMR (CDCl$_3$, 250 MHz): δ 1.17−1.44 (m, 60H, —OCH$_2$CH$_2$—(C*H*$_2$)$_5$—), 1.52−1.70 (m, 12H, —OCH$_2$C*H*$_2$—), 1.94−2.06 (m, 12H, —C*H*$_2$—CH═), 3.82−3.92 (m, 12H, —OC*H*$_2$—), 4.85−5.01 (m, 12H, ═C*H*$_2$), 5.69−5.85 (m, 6H, —C*H*═CH$_2$). ^{13}C NMR (CDCl$_3$, 250 MHz): δ 25.9, 29.1, 29.3, 29.5, 29.6, 30.5, 34.0, 66.0, 114.4, 139.3. ^{31}P NMR (CDCl$_3$, 700 MHz): δ 17.85 (s). MALDI-TOF *m*/*z* (%) 1067 (100).

2,2,4,4,6,6-Hexakis-(8-(oxiran-2-yl)-oct-1-oxy)-cyclotriphosphazene (5). Synthetic procedure followed that for compound **2** to afford **5** as slightly orange, viscous oil in 78% yield (column chromatography, *n*-hexane/ethyl acetate, 10/1, v/v, passing over to pure ethyl acetate, $R_{f,n\text{-hexane/ethylacetate},5/1}$ = 0.2). ^{1}H NMR (CDCl$_3$, 250 MHz): δ 1.18−1.71 (m, 84H, −OCH$_2$−(C*H*$_2$)$_7$−), 2.44 (dd, 6H, ^2J = 5.2, ^3J = 2.6, −CH−(−O−)−C*H*$_2$), 2.73 (dd, 6H, ^2J = 5.1, ^3J = 4.0, −CH−(−O−)−C*H*$_2$), 2.82−2.92 (m, 6H, −C*H*−(−O−)−CH$_2$), 3.79−3.95 (m, 12H, −OC*H*$_2$−). ^{13}C NMR (CDCl$_3$, 250 MHz): δ 25.9, 26.2, 29.4, 29.6, 29.7, 30.5, 32.7, 47.3, 52.6, 66.0. ^{31}P NMR (DMSO, 700 MHz): δ 17.25 (s).

2,2,4,4,6,6-Hexakis-(4-(8-octoxy)-1,3-dioxolan-2-one)-cyclotriphosphazene (6). Synthetic procedure followed that for compound **3** to afford **6** as slightly yellow, viscous oil (column chromatography, *n*-hexane/ethyl acetate, 4/1, v/v, R_f = 0.55, 75% yield). ^{1}H NMR (CDCl$_3$, 250 MHz): δ 1.17−1.53 (m, 60H, —OCH$_2$CH$_2$—(C*H*$_2$)$_5$—), 1.54−1.82 (m, 24H, —OCH$_2$C*H*$_2$—, —C*H*$_2$CH—(O(C═O)O)—CH$_2$), 3.87 (m, 12H, —OC*H*$_2$—), 4.05 (dd, 6H, ^2J = 8.3, ^3J = 7.1, —CH—(O(C═O)O)—C*H*$_2$), 4.52 (dd, 6H, ^2J = 8.2, ^3J = 7.1, —CH—(O(C═O)O)—C*H*$_2$), 4.64−4.75 (m, 6H, —C*H*—(O(C═O)O)—CH$_2$). ^{13}C NMR (CDCl$_3$, 250 MHz): δ 24.6, 25.9, 29.3, 29.5, 30.4, 34.1, 66.0, 69.6, 77.3, 155.4. ^{31}P NMR (CDCl$_3$, 700 MHz): δ 17.22 (s). MALDI-TOF *m*/*z* (%) 1426 (100).

2,2,4,4,6,6-Hexakis-(cis-5-octenyl-1-oxy)-cyclotriphosphazene (7). Synthetic procedure followed that for compound **1** to afford **7** as colorless, viscous liquid (column chromatography, methylene chloride, R_f = 0.85, 89% yield). ^{1}H NMR (CDCl$_3$, 250 MHz): δ 0.91 (t, 18H, ^3J = 7.3, —C*H*$_3$), 1.31−1.46 (m, 12H, —OCH$_2$C*H*$_2$—), 1.54−1.70 (m, 12H, —OCH$_2$CH$_2$C*H*$_2$—), 1.92−2.06 (m, 24H, —C*H*$_2$—CH═CH—C*H*$_2$—), 3.83−3.92 (m, 12H, -OC*H*$_2$-), 5.20−5.40 (m, 12H, −CH$_2$−C*H*=C*H*-CH$_2$−). ^{13}C NMR (CDCl$_3$, 250 MHz): δ 14.5, 20.7, 26.0, 26.8, 30.0, 65.8, 128.8, 132.2. ^{31}P NMR (CDCl$_3$, 700 MHz): δ 18.56 (s). MALDI-TOF *m*/*z* (%) 898 (100).

2,2,4,4,6,6-Hexakis-(4-(3-ethyloxiran-2-yl)-but-1-oxy)-cyclotriphosphazene (8). Synthetic procedure followed that for compound **2** to afford **8** after column chromatography (methylene chloride/ethyl acetate, R_f = 0.85) as slightly yellow, highly viscous oil in 82% yield. ^{1}H NMR (DMSO, 250 MHz): δ 0.89−1.02 (t, 18H, ^3J = 7.3, −C*H*$_3$), 1.35−1.73 (m, 48H, −C*H*$_2$CH$_3$, −OCH$_2$−(C*H*$_2$)$_3$−), 2.74−2.90 (m, 12H, −C*H*−(−O−)−C*H*−C$_2$H$_5$), 3.74−3.90 (m, 12H, −OC*H*$_2$−). ^{13}C NMR (DMSO, 250 MHz): δ 10.5, 20.6, 22.5, 26.6, 29.5, 56.0, 57.1, 64.9. ^{31}P NMR (DMSO, 700 MHz): δ 18.81 (s). MALDI-TOF *m*/*z* (%) 994 (32), 1016 (Na$^+$-Peak, 32), 1032 (K$^+$-Peak, 100).

2,2,4,4,6,6-Hexakis-(4-ethyl-5-(4-butoxy)-1,3-dioxolan-2-one)-cyclotriphosphazene (9). Chlorocobalt tetraphenylporphyrin ((TPP)Co^{III}Cl) catalyst was synthesized following a reported procedure.[20−22] A stainless steel autoclave (250 mL) was charged with a solution of **8** (0.50 g, 0.50 mmol), (TPP)Co^{III}Cl (2 mol %) and *N*,*N*-dimethylaminopyridine (DMAP, 4 mol %) in 15 mL methylene chloride. After purging with nitrogen, the reaction was started by pressurization of the solution with CO$_2$ up to 50 bar. The mixture was then heated to 100 °C accompanied by a pressure increase to 80 bar and stirred for 72 h at this temperature. The autoclave was allowed to cool to room temperature and excess CO$_2$ was discharged. The mixture was concentrated, and the crude product was purified by column chromatography (ethyl acetate/*n*-hexane, 5/1, v/v, R_f = 0.25). Product **9** was obtained as slightly orange, highly viscous oil (0.42 g, 3.34 mmol, 67% yield). ^{1}H NMR (CDCl$_3$, 250 MHz): δ 1.03 (t, 18H, ^3J = 7.3, —C*H*$_3$), 1.36−1.83 (m, 48H, —C*H*$_2$CH$_3$, —OCH$_2$(C*H*$_2$)$_3$—), 3.90 (br, 12H, —OC*H*$_2$—), 4.13−4.30 (m, 0.72 H, *trans*-CH$_2$—C*H*—(O(C═O)O)—C*H*—C$_2$H$_5$), 4.48−4.72 (m, 11.28 H, *cis*-CH$_2$—C*H*—(O(C═O)O)—C*H*—C$_2$H$_5$). ^{13}C NMR (CDCl$_3$, 250 MHz): δ 10.3, 22.4, 22.5, 28.7, 29.9, 65.7, 80.0, 81.5, 154.9. ^{31}P NMR (CDCl$_3$, 700 MHz): δ 18.57 (s). MALDI-TOF *m*/*z* (%) 1258 (100).

2,2,4,4,6,6-Hexakis-(2-(2-(2-(2-methoxyethoxy)ethoxy)ethoxy)ethoxy)-cyclotriphosphazene (10).[23]. Synthetic procedure followed that for compound **1** to afford **10** as colorless oil (column chromatography, *n*-hexane/THF, 1/3, v/v, R_f = 0.28, 90% yield). ^{1}H NMR (CDCl$_3$, 250 MHz): δ 3.34 (s, 18H, —C*H*$_3$), 3.48−3.54 (m, 12H, P—OCH$_2$C*H*$_2$—), 3.55−3.68 (m, 72H, —O—(C*H*$_2$C*H*$_2$O)$_3$—CH$_3$), 4.00 (br, 12H, P—OC*H*$_2$—). ^{13}C NMR (CDCl$_3$, 250 MHz): δ 59.3, 65.2, 70.2, 70.7, 70.8, 72.1. ^{31}P NMR (CDCl$_3$, 700 MHz): δ 17.11 (s). MALDI-TOF *m*/*z* (%) 1379 (100).

2. HPB-Based Model Compounds

Hexakis-(4-(hept-4-enoate)-phenyl)-benzene (11). 6-Heptenoyl chloride was synthesized following a reported procedure.[24] Hexakis-(4-hydroxyphenyl)-benzene[25] (0.20 g, 0.32 mmol) and dry pyridine (125 mL) were mixed at 60 °C in a Schlenk flask. Under an N$_2$ atmosphere, a solution of 6-heptenoyl chloride (0.56 g, 3.81 mmol) in 5 mL dry acetonitrile was added dropwise at 60 °C under stirring. The temperature was increased to 85 °C, and the mixture was stirred at this temperature for 24 h. Subsequently, 15 mL acetonitrile, 15 mL ethyl acetate, and 15 mL water were added, and the organic phase was washed three times with 10 mL of 15 wt % aqueous sodium carbonate and once with 15 mL water. The combined organic layer was dried over MgSO$_4$, concentrated, and the residue was subjected to column chromatography with *n*-hexane/ethyl acetate (3/1, v/v, R_f = 0.65) as eluent. Product **11** was obtained as a white powder (0.35 g, 0.27 mmol, 84% yield). ^{1}H NMR (CDCl$_3$, 250 MHz): δ 1.35−1.51 (m, 12H, —C*H*$_2$CH$_2$—CH═CH$_2$), 1.57−1.75 (m, 12H, —O—C(═O)—CH$_2$C*H*$_2$—), 1.96−2.13 (m, 12H, —C*H*$_2$—CH═CH$_2$), 2.42 (t, 12H, ^3J = 7.4, —O—C(═O)—C*H*$_2$—), 4.88−5.06 (m, 12H, —CH$_2$—CH═C*H*$_2$), 5.67−5.88 (m, 6H, —CH$_2$—C*H*═CH$_2$), 6.63 (d, 12H, ^3J = 8.7, *ortho*-Ar*H*), 6.74 (d, 12H, ^3J = 8.7, *meta*-Ar*H*). ^{13}C NMR (CDCl$_3$, 250 MHz): δ 24.5, 28.5, 33.6, 34.4, 115.0, 120.3, 132.4, 137.7, 138.6, 140.2, 148.8, 171.8. MALDI-TOF *m*/*z* (%) 1315 (Na$^+$-Peak, 100).

Hexakis-(4-(5-oxiran-2-yl-pentanoate)-phenyl)-benzene (12). **11** (0.35 g, 0.27 mmol) was dissolved in 80 mL methylene chloride. The solution was cooled to 0 °C, and MCPBA (77%, 0.61 g, 2.72 mmol) was added portionwise. The mixture was stirred vigorously for 96 h. After complete epoxidation, the mixture was washed three times with 2 wt % sodium hydroxide solution and water. The organic phase was dried over MgSO$_4$ and then concentrated to dryness. The crude product **12** was obtained as white powder and used without further purification (0.36 g, 0.26 mmol, 96% yield). ^{1}H NMR (CDCl$_3$, 250 MHz): δ 1.40−1.80 (m, 36H, —O—C(═O)—CH$_2$—(C*H*$_2$)$_3$—), 2.36−2.50 (m, 18H, —O—C(═O)—C*H*$_2$—, —CH—(—O—)—CH$_2$), 2.72 (dd, 6H, ^2J = 5.0, ^3J =

4.0, —CH—(—O—)—CH_2), 2.83−2.96 (m, 6H, —CH—(—O—)—CH_2), 6.63 (d, 12H, ^3J = 8.6, *ortho*-ArH), 6.74 (d, 12H, ^3J = 8.6, *meta*-ArH). ^{13}C NMR ($CDCl_3$, 250 MHz): δ 24.8, 25.7, 32.3, 34.4, 47.9, 54.3, 120.3, 132.4, 137.7, 140.2, 148.7, 171.6.

Hexakis-(4-(5-(2-oxo-1,3-dioxolan-4-yl)-pentanoate)-phenyl)-benzene (13). A stainless steel autoclave (250 mL) was charged with a solution of **12** (0.36 g, 0.26 mmol), tetrabutylammonium iodide (0.06 g, 0.16 mmol), and tributyltin iodide (0.07 g, 0.16 mmol) in 50 mL of freshly distilled THF. After purging with nitrogen, the reaction was started by pressurization of the solution with CO_2 up to 50 bar. The mixture was then heated to 80 °C accompanied by a pressure increase to 80 bar and stirred for 120 h at this temperature. The autoclave was allowed to cool to room temperature and excess CO_2 was discharged. The product was precipitated in a minimum amount of ethyl acetate, filtered, and washed with 100 mL chilled methanol, 100 mL chilled hexane, and a small amount of chilled acetone to obtain **13** as a white powder (0.34 g, 0.21 mmol, 79% yield). ^{1}H NMR (DMSO, 250 MHz): δ 1.23−1.81 (m, 36H, —O—C(=O)—CH_2—(CH_2)$_3$—), 2.41−2.53 (m, 12H, —O—C(=O)—CH_2—), 4.11 (dd, 6H, ^2J = 8.0, ^3J = 7.3, —CH—(O(C=O)O)—CH_2), 4.55 (dd, 6H, ^2J = 8.0, ^3J = 7.2, —CH—(O(C=O)O)—CH_2), 4.68−4.88 (m, 6H, —CH—(O(C=O)O)—CH_2), 6.66 (d, 12H, ^3J = 8.3, *ortho*-ArH), 6.87 (d, 12H, ^3J = 8.3, *meta*-ArH). ^{13}C NMR (DMSO, 250 MHz): δ 23.6, 23.8, 32.5, 33.2, 69.2, 76.9, 120.0, 131.8, 137.1, 139.7, 148.1, 154.9, 171.0.

Hexakis-(4-(undec-10-enoate)-phenyl)-benzene (14). Synthetic procedure followed that for compound **11** to afford product **14** as colorless oil (column chromatography, *n*-hexane/THF, 4/1, v/v, R_f = 0.53, 78% yield). ^{1}H NMR ($CDCl_3$, 250 MHz): δ 1.18−1.41 (m, 60H, —O—C(=O)—(CH_2)$_2$—(CH_2)$_2$—, —(CH_2)$_3$—CH_2—CH=CH_2), 1.56−1.72 (m, 12H, —O—C(=O)—CH_2CH_2—), 1.97−2.05 (m, 12H, —CH_2—CH=CH_2), 2.40 (t, 12H, ^3J = 7.1, —O—C(=O)—CH_2—), 4.86−5.03 (m, 12H, —CH_2—CH=CH_2), 5.70−5.87 (m, 6H, —CH_2—CH=CH_2), 6.63 (d, 12H, ^3J = 8.7, *ortho*-ArH), 6.74 (d, 12H, ^3J = 8.7, *meta*-ArH). ^{13}C NMR ($CDCl_3$, 250 MHz): δ 25.0, 29.1, 29.3, 29.4, 29.5, 34.0, 34.6, 114.4, 120.3, 132.4, 137.7, 139.4, 140.2, 148.8, 172.0. MALDI-TOF *m*/*z* (%) 1628 (10), 1651 (Na^+-Peak, 100).

Hexakis-(4-(9-oxiran-2-yl-nonanoate)-phenyl)-benzene (15). Synthetic procedure followed that for compound **12** to afford product **15** as white powder (95% yield). ^{1}H NMR ($CDCl_3$, 250 MHz): δ 1.18−1.71 (m, 84H, —O—C(=O)—CH_2—(CH_2)$_7$—), 2.35−2.45 (m, 18H, —O—C(=O)—CH_2—, —CH—(—O—)—CH_2), 2.68−2.74 (dd, 6H, ^2J = 5.1, ^3J = 3.9, —CH—(—O—)—CH_2), 2.82−2.91 (m, 6H, —CH—(—O—)—CH_2), 6.61 (d, 12H, ^3J = 8.6, *ortho*-ArH), 6.73 (d, 12H, ^3J = 8.6, *meta*-ArH). ^{13}C NMR ($CDCl_3$, 250 MHz): δ 25.0, 26.1, 29.3, 29.4, 29.5, 29.6, 32.7, 34.5, 47.3, 52.7, 120.3, 132.4, 137.7, 140.2, 148.8, 172.0. MALDI-TOF *m*/*z* (%) 1746 (Na^+-Peak, 100), 1762 (K^+-Peak, 60), 1786 (Na^+/K^+-Peak, 33).

Hexakis-(4-(9-(2-oxo-1,3-dioxolan-4-yl)nonanoate)-phenyl)-benzene (16). Synthetic procedure followed that for compound **13** to afford product **16** as white powder (77% yield). ^{1}H NMR ($CDCl_3$, 250 MHz): δ 1.21−1.86 (m, 84H, —O—C(=O)—CH_2—(CH_2)$_7$—), 2.41 (t, 12H, ^3J = 7.4, —O—C(=O)—CH_2—), 4.05 (dd, 6H, ^2J = 8.0, ^3J = 7.2, —CH—(O(C=O)O)—CH_2), 4.50 (dd, 6H, ^2J = 8.1, ^3J = 7.2, —CH—(O(C=O)O)—CH_2), 4.60−4.75 (m, 6H, —CH—(O(C=O)O)—CH_2), 6.62 (d, 12H, ^3J = 8.6, *ortho*-ArH), 6.74 (d, 12H, ^3J = 8.6, *meta*-ArH). ^{13}C NMR ($CDCl_3$, 250 MHz): δ 24.6, 24.9, 29.1, 29.2, 29.3, 34.1, 34.5, 69.6, 77.4, 120.3, 132.4, 137.8, 140.4, 148.8, 155.3, 171.9. EA (%): calc. C 68.86; H 6.99. Found: C 68.78; H 6.91.

Hexakis-(4-(2-(2-(2-(2-methoxyethoxy)ethoxy)ethoxy)ethoxy)-phenyl)-benzene (19). Compound **19** was prepared following a reported procedure: 1-(2-(2-(2-(2-methoxyethoxy)ethoxy)ethoxy)ethoxy)-4-bromobenzene (**17**) is formed by reacting 2-(2-(2-(2-methoxyethoxy)ethoxy)ethoxy)ethyl-4-methylbenzensulfonate with 4-bromophenol in presence of anhydrous K_2CO_3 in DMF.[26,27] A one-pot *Sonogashira* reaction of **17** provides 1,2-bis(4-(2-(2-(2-(2-methoxyethoxy)ethoxy)ethoxy)-ethoxy)phenyl)ethyne (**18**).[28] After subsequent one-pot cyclotrimerization of **18** product **19** is obtained as colorless oil (overall yield 32%).[25,26] ^{1}H NMR ($CDCl_3$, 300 MHz): δ 3.33 (s, 18H, −CH_3), 3.49−3.55 (m, 12H, CH_2−OCH_3), 3.58−3.68 (m, 60H, −O(CH_2-CH_2O)$_2$−OCH_2CH_2−OCH_3), 3.69−3.75 (m, 12H, Ar−O−CH_2CH_2−), 3.86−3.93 (m, 12H, Ar−O−CH_2−), 6.37 (d, 12H, ^3J = 8.7, *ortho*-ArH), 6.60 (d, 12H, ^3J = 8.7, *meta*-ArH). ^{13}C NMR ($CDCl_3$, 300 MHz): δ 59.2, 67.1, 70.0, 70.7, 70.9, 113.1, 132.5, 133.8, 140.4, 156.1. MALDI-TOF *m*/*z* (%) 1171 (100), 1793 (Na^+-Peak, 14), 1809 (K^+-Peak, 14).

RESULTS AND DISCUSSION

Model Compound Synthesis. The synthetic route employed to prepare 2-oxo-1,3-dioxolane substituted model compounds based on CTP is following a three step reaction (Scheme 1a): First, $N_3P_3Cl_6$ is reacted with the appropriate sodium alkoxide of ω-hexen-1-ol (**1**) or ω-decen-1-ol (**4**), respectively, followed by epoxidation with 3-chloroperoxybenzoic acid (MCPBA) to yield hexakis-(4-(oxiran-2-yl)but-1-oxy)-cyclotriphosphazene (**2**) and hexakis-(8-(oxiran-2-yl)oct-1-oxy)-cyclotriphosphazene (**5**). It is essential to use *equimolar* rather than catalytic amounts of the antioxidant 2,6-ditert-butyl-4-methylphenol (BHT) referred to the amount of MCPBA to prevent serious degradation of the CTP.[29] In the final step, **2** and **5** are converted into hexakis-(4-(4-butoxy)-1,3-dioxolan-2-one)-cyclotriphosphazene (**3**) and hexakis-(4-(8-octoxy)-1,3-dioxolan-2-one)-cyclotriphosphazene (**6**) by transition metal catalyzed insertion of CO_2 into the epoxide ring.[30]

In order to obtain an ethyl-substituted cyclocarbonate, alcoholate **7** was used. The CO_2 insertion into the internal *cis*-epoxide **8** using tributyltin iodide/tetrabutylammonium iodide as catalyst system was not exceeding 80% of conversion, as evidenced by ^{1}H NMR, despite a higher reaction temperature of 100 °C compared to the terminal epoxides and an applied CO_2 partial pressure of 95 bar. Alternatively, lithium bromide applied in combination with *n*-methyl pyrrolidone under similar reaction conditions than described before resulted also only in a partial conversion of about 90%.[31] However, a rather rarely reported full conversion of CO_2 insertion into the internal epoxide was achieved in an autoclave using the more efficient catalyst system consisting of 2 mol % chlorocobalt tetraphenylporphyrin ((TPP)$4Co^{III}Cl$) and 4 mol % dimethylaminopyridine (DMAP).[20−22] The commercially available Co^{II}-tetraphenylporphyrin was not sufficient due to the limited catalytic activity compared to oxidized (TPP)$Co^{III}Cl$.[22] In our case, the product cis:trans ratio for (TPP)$Co^{III}Cl$/DMAP amounts to 94:6, supporting the proposed mechanistic pathway from Paddock et al., which suggests retention of the configuration due to double inversion of the stereochemistry at the attacked carbon.[22] In contrast, for the partially converted product using the catalyst system Bu_4NI/Bu_3SnI mainly inversion of the configuration occurs as the product cis:trans ratio was 20:80.

CTP-based model compounds with alternative side groups containing less oxygen atoms, e.g. lactone side groups, were not accessible starting from the epoxy functionalized substances **2** and **5**. Rather, full conversion was not achieved following a modified procedure applying 1-morpholino-2-trimethylsilyl acetylene and $BF_3 \cdot OEt_2$,[32] or the reaction conditions were too harsh in terms of the elevated temperature as for e.g. the reaction of the epoxides **2** and **5** with diethylmalonate.[33] Consequently,

Scheme 1. (a) Synthesis of Cyclic Carbonate and Oligo(oxyethylene) Functionalized Model Compounds Based on a CTP Core and (b) Synthesis of Cyclic Carbonate and Oligo(oxyethylene) Functionalized Model Compounds Based on an HPB Core

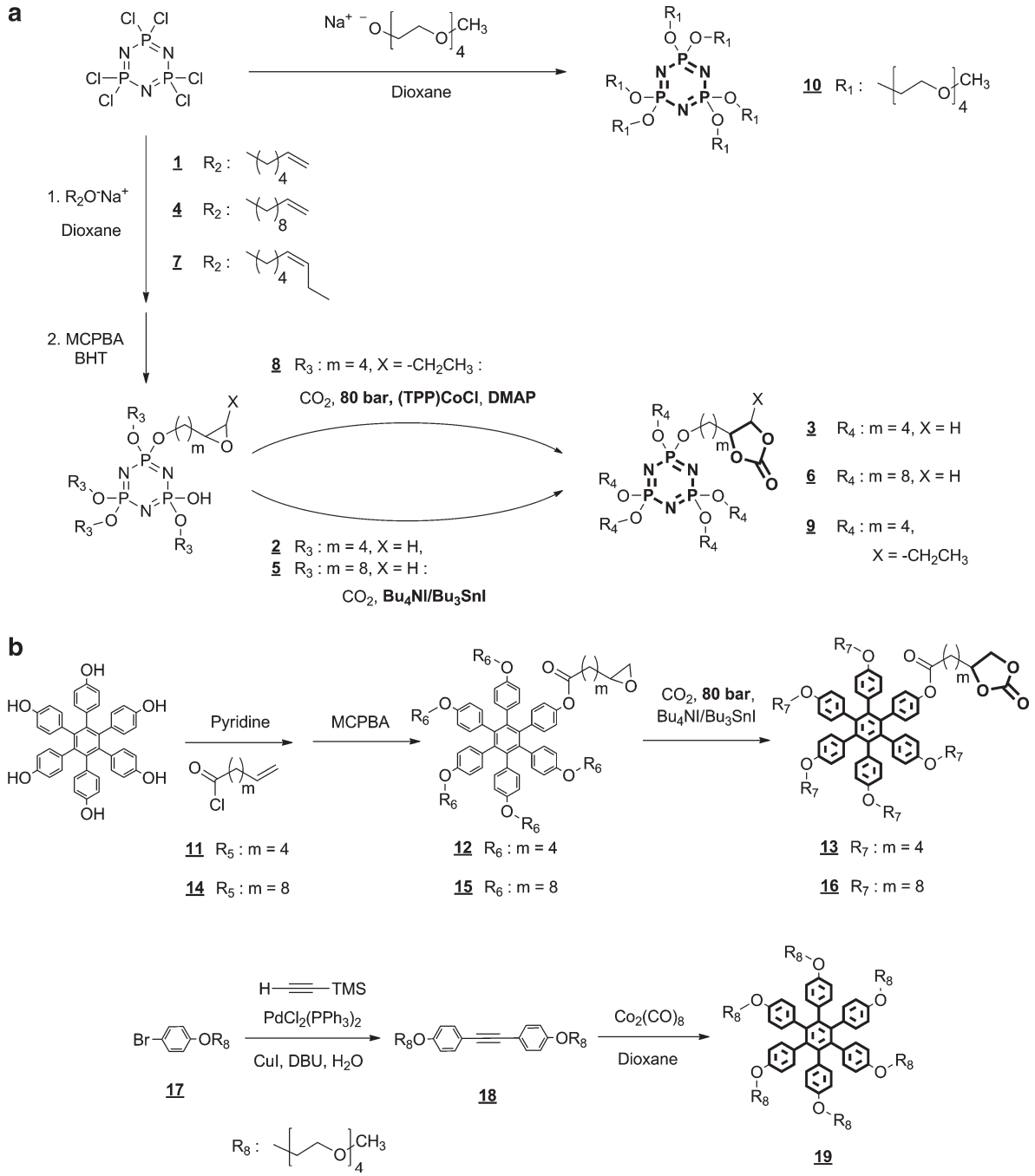

significant degradation of the phosphazene ring was observed, notable by several peaks around 0 ppm in the corresponding ^{31}P NMR spectra.

The synthesis route for the HPB-based model compounds started from hexakis-(4-hydroxyphenyl)-benzene (Scheme 1b).[25]

Hexakis-(4-(hept-4-enoate)-phenyl)-benzene (**11**) and hexakis-(4-(undec-10-enoate)-phenyl)-benzene (**14**) were synthesized via esterification of 6-heptenoyl chloride and 10-undecenoyl chloride respectively with hexakis-(4-hydroxyphenyl)-benzene in the presence of pyridine. The build-up of the cyclic carbonate side group followed a similar way described above for the CTP model compounds. It is essential that the esterification is performed prior to epoxidation, since otherwise the basic reaction conditions of the esterification lead to epoxide ring-opening and subsequent formation of *trans*-1,2-dioles. In both cases, moreover, complete transition metal catalyzed CO_2 insertion was successful only at a CO_2 partial pressure of about 80 bar at 80 °C.

Attempts to synthesize an HPB-based model compound with a shorter alkyl spacer, e.g. in order to allow for a higher stacking probability of the HPB moieties, proved difficult due to limited solubility. Since the resulting product out of the reaction of hexakis-(4-hydroxyphenyl)-benzene and epichlorhydrin was

dx.doi.org/10.1021/cm103559d |*Chem. Mater.* 2011, 23, 2120–2129

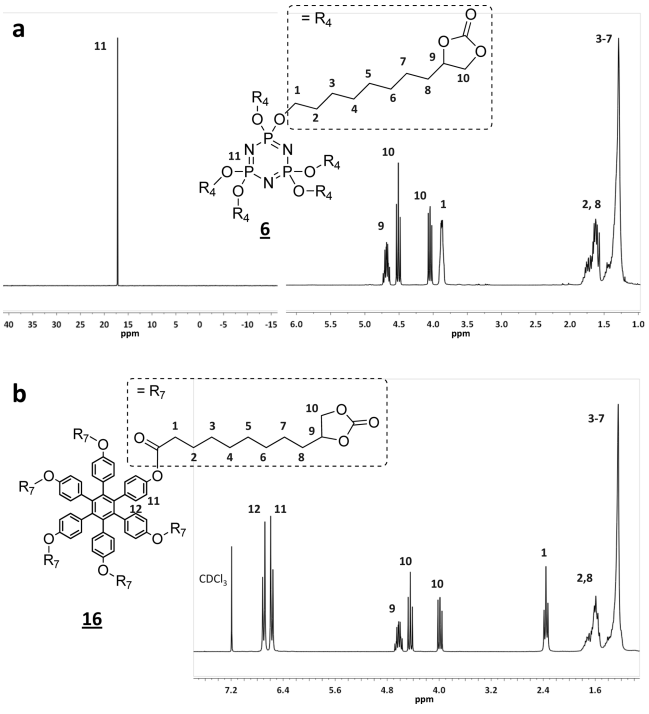

Figure 1. (a) ^{31}P NMR (left) and ^{1}H NMR spectra (right) of CTP model compound **6**. (b) ^{1}H NMR spectrum of HPB model compound **16**.

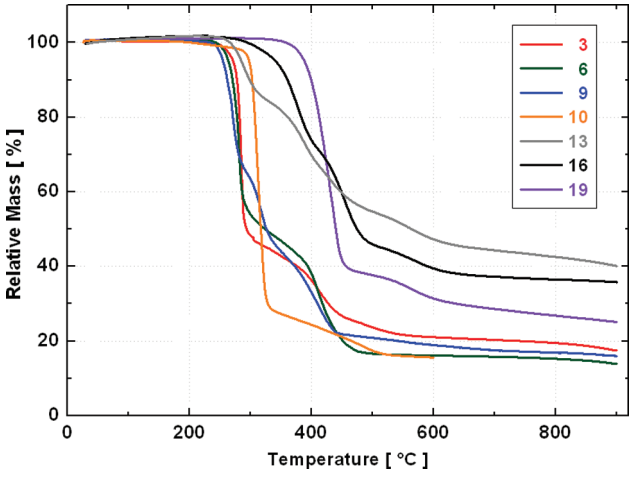

Figure 2. TGA traces of the pure model compounds under N_2 at a constant heating rate of 10 K min^{-1}.

hardly soluble in any common solvent, for the pressurized CO_2 insertion, only a limited degree of conversion (≈67%, verified by elemental analysis) was achieved.[34] This also applies for the reaction pathway starting from hexakis-(4-hydroxyphenyl)-benzene and 4-pentenoyl chloride.

For both model compound series, an oligo(oxyethylene) functionalized reference was synthesized (**10** and **19**).

Model Compound Characterization. All model compounds are soluble in THF, dioxane or DMF. Characterization after purification and drying in vacuum by ^{1}H, ^{13}C, and ^{31}P NMR spectroscopy revealed well-defined, completely functionalized, and highly pure products. Figure 1a shows the representative

Scheme 2. Proposed Mechanism for the Thermal Induced Rearrangement of the Cyclotriphosphazene Side Groups[35]

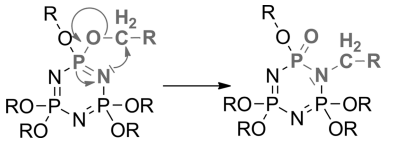

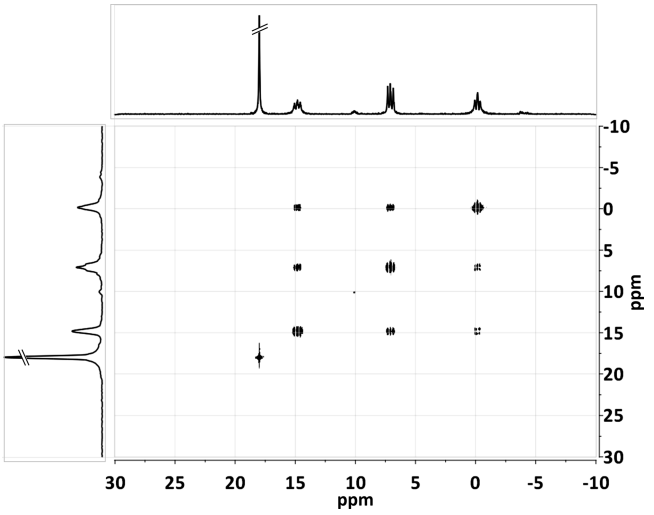

Figure 3. ^{31}P−^{31}P COSY NMR of model compound **6** after heating for 72 h at 100 °C in DMSO.

^{1}H and ^{31}P NMR spectra of hexakis-(4-(8-octoxy)-1,3-dioxolan-2-one)-cyclotriphosphazene (**6**). Similar to all CTP-based model compounds, the ^{31}P NMR of **6** exhibits a sharp singlet at +17.22 ppm, proving that only equivalent phosphorus atoms exist in the CTP core in agreement with a fully substituted phosphazene ring. The ^{1}H NMR spectra confirm the chemical structure, which were further approved by ^{13}C NMR and MALDI mass spectrometry.

Thermal Properties. All model compounds were stable up to at least 250 °C when investigated by TGA under N_2 applying a heating rate of 10 K min^{-1} (Figure 2). The onset of decomposition in case of the CTP model compounds bearing cyclic carbonate units is at around 250 °C ± 5 °C, whereas the oligo(oxyethylene) functionalized equivalent **10** is even stable up to 300 °C, indicating, that the cyclic carbonate decomposes most likely before the phosphazene ring does. Model compounds based on HPB cores (**13** and **16**) appear to be slightly more stable compared to the CTPs. Similar to the CTP analogues, the oligo(oxyethylene) functionalized HPB model compound **19** is less sensitive to heat. The thermal stability of the considered blends with lithium bis-(trifluoromethanesulfone)imide (LiTFSI) for the particular compounds was comparable.

It is important to note that for the CTP model compounds, a rearrangement of the side groups could be observed after extensive heating at temperatures above 80 °C. The rearrangement follows the proposed mechanism shown in Scheme 2 as evidenced by ^{31}P NMR.[35]

After heat treatment, the ^{31}P−^{31}P COSY NMR (Figure 3) shows three multiplets at around +15, +7, and 0 ppm which are not present in the initial sample. Strong ^{2}J and ^{4}J coupling between the three phosphorus nuclei can be observed. The splitting pattern is

dx.doi.org/10.1021/cm103559d |*Chem. Mater.* 2011, 23, 2120–2129

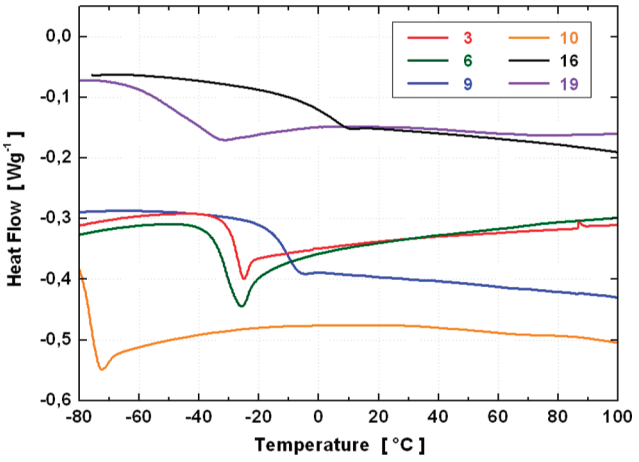

Figure 4. DSC traces (second heating) of the pure model compounds under N_2 at a constant heating rate of 10 K min^{-1}.

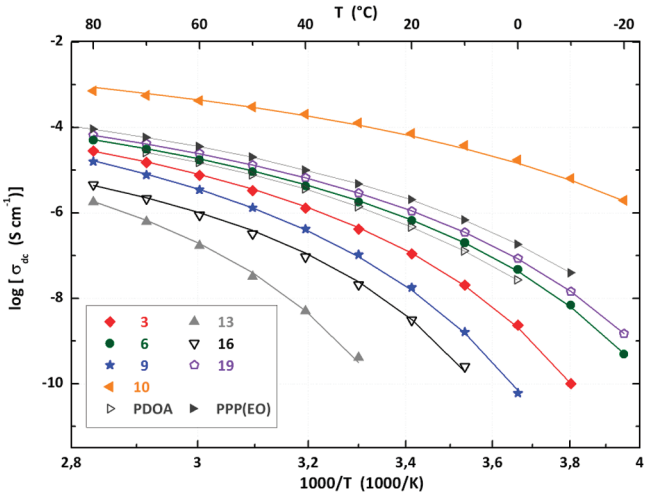

Figure 5. Arrhenius plot of the temperature dependent conductivity of the model compounds blended with LiTFSI (molar ratio Li:O = 1:50, except for PDOA: Li:O = 1:16.6). The lines through the measured data points represent the WLF fits.

in each case a double doublet due to the coupling of the particular phosphorus nucleus with the remaining two magnetic nonequivalent phosphorus nuclei in the cycle. The NMR data indicate that the CTP core remains intact, while the substitution pattern may be a matter of the samples thermal history.

Differential scanning calorimetry (DSC) was used to study thermal transitions of the model compounds, whereby second heating profiles were compared. At a heating rate of 10 K min^{-1}, apparent glass transitions (T_g) were observed for all CTP-based substances (Figure 4).

The thermal behavior of the HPB-based model compounds is more difficult to address, since the thermal transitions are very much kinetically controlled. Whereas pure **13** shows a sharp, reproducible melting transition at 152 °C, the equivalent model compound **16** bearing a longer alkyl spacer shows a melting peak at 58 °C just in the first heating scan. Further heating and cooling scans exhibit a glass transition at 3.5 °C only, where even prolonged annealing for several hours at 15 °C did not lead to partial crystallization.

The T_g's of the model compounds cover a broad temperature range. The T_g of the pure CTP model compound **3** is −28.9 °C. An increase of the side chain length may induce a greater free volume; hence the onset of segmental motion and the glass transition is shifted to lower temperatures. Consequently, compound **6** exhibits a slightly lower T_g as compared to compound **3**. The T_g of the model compound **9** with the internal 2-oxo-1,3-dioxolane group is higher, probably because the mobility of the side chain is decreased as compared to the mobility of the side chains in compounds **3** and **6**.

Adding LiTFSI to the CTP-based model compounds increases the glass transition temperatures with increasing lithium salt concentration. In contrast, the glass transition temperature of the HPB-based model compound **16** decreases slightly upon addition of LiTFSI. Besides, the blend of **13** with LiTFSI does not show a melting peak as pure **13** does but instead a glass transition well below the melting peak of pure compound **13**.

This raises the question of the nature of the observed glass transitions. While in the CTP-based models both core and side chains are rather flexible and may be involved in the glass transition, in the HPB-based models the core is rather stiff and merely the onset of the side chain motion appears to fit the relatively low glass transition temperatures of the blends. In both cases, a thorough analysis of the nature of the glass transition and more important the molecular basis of lithium ion transport by solid state NMR is currently in progress. These studies potentially allow for a more rational understanding of molecular dynamics within the matrix and qualify for structure−property correlation in such kind of electrolytes. The results will be discussed in a forthcoming publication.

The oligo(oxyethylene) functionalized model compounds **10** and **19** exhibit lower glass transition temperatures than the cyclic carbonate analogues, probably due to the higher mobility of the oligo(oxyethylene) side groups and their weaker electrostatic interactions compared to the more polar 2-oxo-1,3-dioxolane functionalities.

Notably, all blends discussed in this work have been investigated in the amorphous state, which was confirmed based on X-ray diffraction data.

Ionic Conductivity. At 40 °C, the ionic conductivities of the homogeneous blends of the model compounds with LiTFSI reach 4.3×10^{-6} S cm^{-1} in the case of hexakis-(4-(8-octoxy)-1,3-dioxolan-2-one)-cyclotriphosphazene (**6**) and 8.9×10^{-8} S cm^{-1} for the respective HPB model **16**, each at a molar Li:O ratio of 1:50. The observable bulk conductivity of the model compounds apparently scales with the spacer length, since the conductivity decreases from models **6** to **3** and **16** to **13**, respectively, when the appropriate model compounds with longer and shorter alkyl spacers between core and the lithium ion solvating 2-oxo-1,3-dioxolane groups are compared (Figure 5).

The oligo(oxyethylene) functionalized references **10** and **19** exhibit conductivities which exceed the ionic conductivities of the 2-oxo-1,3-dioxolane functionalized analogues by about 2 orders of magnitude. This corresponds to the clearly lower glass transition temperatures of these models (Table 1).

Interestingly, the conductivity of the CTP-based model compound **9** with an ethyl-substituted cyclic carbonate exhibits an even lower conductivity as its appropriate counterpart, model compound **3** with unsubstituted cyclic carbonate. Obviously, the ethyl side group at the carbonate cycle does not cause a weaker interaction between the solvating moieties and the Li-ions.

In relation to the polymer which we studied earlier (poly(2-oxo-1,3-dioxolan-4-yl)methyl acrylate, PDOA, T_g = 327 K),[12]

dx.doi.org/10.1021/cm103559d |*Chem. Mater.* 2011, 23, 2120–2129

Table 1. Apparent Glass Transition Temperatures, log σ (at 40 °C), and the Calculated WLF Parameters C_1 and C_2 for the Model Compounds Blended with LiTFSI in a Molar Ratio Li:O = 1:50

model compound[a]	$T_{ref} = T_g$ (°C)	log σ (40 °C) (S cm^{-1})	C_1	C_2 (K)	R^{2b}
3	−18.4	−5.89	24.02	49.35	0.999
6	−34.1	−5.37	24.29	52.63	0.999
9	−12.1	−6.38	27.10	48.27	0.999
10	−61.6	−3.69	20.96	58.52	0.997
13	+12.7	−8.30	26.56	39.46	0.998
16	+2.3	−7.05	22.30	44.44	0.999
19	−39.2	−5.18	25.02	50.76	0.999

[a] See the Experimental Section or Scheme 1a and b for sample numbering. [b] R^2 is the correlation coefficient obtained between linear fit and experimental data by plotting $(T - T_g)/\log(\sigma/\sigma(T_g))$ vs $T - T_g$.

the phosphazene model **9** is showing only slightly higher ionic conductivity despite the much lower T_g (Table 1). This is consistent with the fact that, for PDOA, the reference temperature in a WLF-treatment is found to have values more than 100 K below the actual T_g. The EO-functionalized HPB-based model **19** compares very well with poly(*p*-phenylene) bearing oligo(oxyethylene) side chains (PPP(EO)) with respect to conductivity. This is rather surprising, since PPP(EO) consists of a stiff main chain layer embedded in an amorphous matrix of the EO side chain segments exhibiting a nanophase separated structure.[13] However, only the EO side chains were found to contribute to the conductivity in PPP(EO), and therefore, conductivity of **19** is in a similar range.

The temperature dependent DC conductivity of the various model compounds blended with LiTFSI (Figure 5) does not follow simple Arrhenius law, since a $\log(\sigma) \sim T^{-1}$ behavior cannot be observed. However, William−Landel−Ferry (WLF) type behavior is found, which is related to the free volume theory. Experimental conductivity data obey the WLF equation:

$$\sigma(T) = \sigma(T_0) \exp \frac{C_1(T - T_{ref})}{C_2 + (T - T_{ref})} \quad (1)$$

In eq 1 $\sigma(T)$ is the ionic conductivity at a given temperature T, T_{ref} is the reference temperature, and C_1 and C_2 are two parameters containing the temperature dependence of the observable ionic conductivity, which can be derived from the experimental data simply by plotting $(T - T_g)/\log(\sigma(T)/\sigma(T_g))$ versus $T - T_g$. For all model compound blends, the observed glass transition temperatures T_g serve as reference temperature T_{ref}. The data are displayed in Table 1. Especially the C_1 values are similar for all considered compounds and are fairly close to the universal value of C_1 = 17.4.[36] C_2 carries information on the "character" of the compound (universal C_2 = 51.6 K),[36] including the presence of different side groups and/or cores. The full lines through the data points shown in Figure 5 represent the respective total fits. In addition, based on this data, a plot of $\log(\sigma)$ versus $(T - T_g)$ is leading to a master curve, where the experimental ionic conductivity data of the blends with LiTFSI fall together within limits of error (Figure 6), except for the blended oligo(oxyethylene) functionalized CTP **10**.

The fitting curve of compound **10** is shifted along the *y*-axis about 1 order of magnitude, in contrast to the HPB-based counterpart **19**, which matches the master curve. The reason

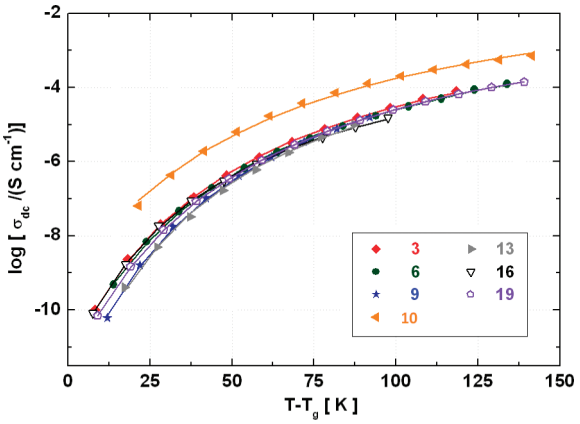

Figure 6. WLF master curve of the temperature dependent conductivity of the model compounds blended with LiTFSI (molar ratio Li:O = 1:50) vs the reduced temperature $T - T_g$.

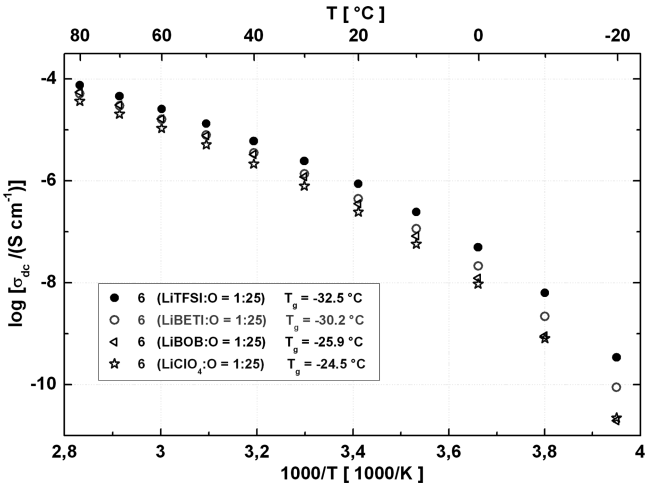

Figure 7. Temperature dependent ionic conductivity of the model compound **6** blended with different lithium salts with different sized counterions (molar ratio Li:O = 1:25).

for this differential behavior yet is currently unclear but may be related to a different nature of the glass transition.

Notably, variation of the lithium salt had no significant influence on the ionic conductivity of the CTP model compounds, which implies, that the CTP models are suitable lithium ion solvents for various lithium salts, irrespective of the salt dissociation constants and counterion sizes. Figure 7 shows the ionic conductivity of model compound **6** blended with LiTFSI, lithium perchlorate ($LiClO_4$), lithium bis(pentafluoroethanesulfone)imide (LiBETI), and lithium bis(oxalate) borate LiBOB), each in molar ratio Li:O = 1:25.

The ionic conductivity differs in the low temperature regime about 1 order of magnitude, which can be associated with variations of the glass transition temperature of the appropriate blends. The observable differences decrease with increasing temperature simply because the influence of T_g on conductivity decreases with increasing temperature. Thus, the blend with $LiClO_4$ exhibits the highest T_g but the lowest ionic conductivity. For the HPB-based model compounds, blends of compound **16** with $LiClO_4$ or LiBOB gave no fully homogeneous mixtures in contrast to the ones with LiTFSI, illustrating the well-known

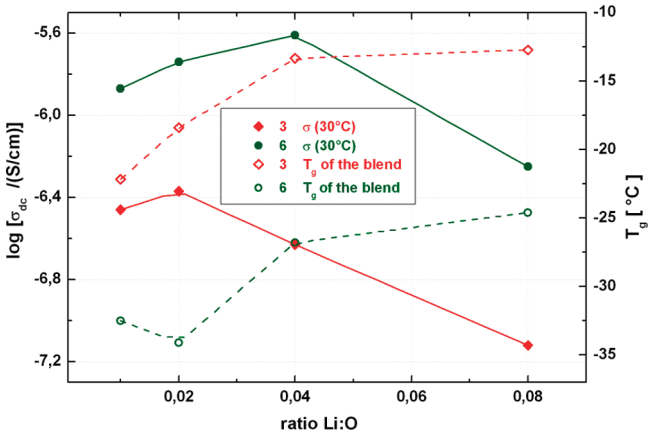

Figure 8. Ionic conductivity at 30 °C and related glass transition temperatures of the model compounds **3** and **6** blended with LiTFSI as a function of molar ratio Li:O.

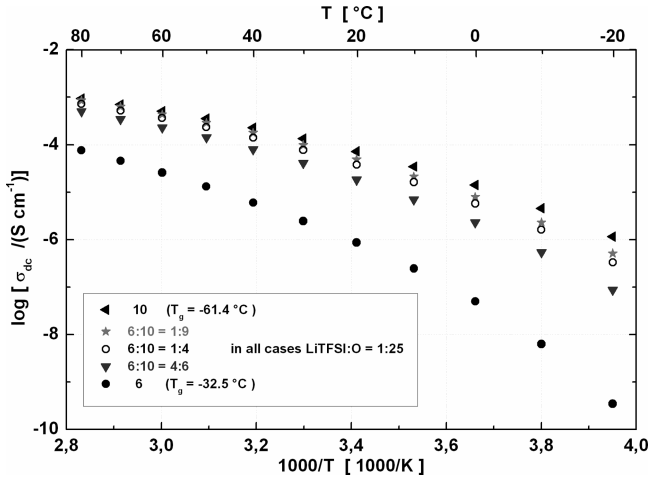

Figure 9. Temperature dependent ionic conductivity of the model compounds **6** and **10** in different mixing ratios blended with LiTFSI (molar ratio Li:O = 1:25).

plasticizing effect of LiTFSI.[37] On the basis of these results, blends with LiTFSI were chosen for further measurements on the HPB models.

The dependence of the ionic conductivity of the blends containing compounds **3** and **6** on the LiTFSI concentration is shown in Figure 8. Furthermore, the development of the glass transition temperatures is mapped.

The ionic conductivity exhibits a maximum for both blends, while the glass transition temperatures increase with increasing salt concentration. Since the ionic conductivity is proportional to the number of effective charge carriers n_i, their mobility q_i, and the electric charge u_i,[38] at low salt contents, the increase of charge carriers is apparently responsible for an increase in conductivity. The potentially displaced counteracting effect of an increase in the glass transition temperature due to cation complexation and ion−dipole interactions causes the observed maxima in ionic conductivity. Due to the lower glass transition and most likely enhanced system mobility of pure compound **6** over **3**, the optimum molar Li:O ratio for maximum ionic conductivity is 1:25 for **6** compared to 1:50 in the case of **3**. Similar studies have been recently described for low-T_g (ca. −80 °C) cyclosiloxane blends.[39]

Since a higher ion mobility and improved salt dissociation is expected in oligo(oxyethylene) functionalized substances as compared to cyclic carbonate functionalized models, mixtures of models **6** and **10** were studied (Figure 9).

For all blends, the conductivity values did not exceed the values obtained for the pure oligo(oxyethylene) model compound **10**. This is in contrast to results reported by West et al. for hybrid polysiloxanes bearing EO and cyclic carbonate side chains.[40] In the present case, no depression of the glass transition temperatures as a result of blending could be observed. Identical results were obtained for the mixtures of the respective HPB model compounds **16** and **19**.

Nevertheless, the absolute conductivity values of the cyclic carbonate functionalized model compounds exhibit relatively low values even at 40 °C, despite the comparatively low glass transition temperatures. While for the HPB models, the elevated glass transition temperatures appear to be the predominant factor for the diminished ionic conductivity, for the low-T_g CTP models, the results suggest that the interaction of the lithium ions with the solvating 2-oxo-1,3-dioxolane moieties is actually too strong. This conclusion is also supported by the conductivity data of the previously mentioned open chain polymer PDOA (Figure 5). In order to understand the discrepancy between low glass transition temperatures and low conductivity values entirely, it is essential to get a closer insight into the complex interplay between the mobility of the side groups and their interactions with the lithium ions. In consideration of what is known about the solvation shell of the lithium ions and the transport mechanism, the lithium ion exchange between solvating moieties can be described as being linked to local rotations of the terminal groups. In the present case, still, at ambient temperatures, those motion modes are supposed to be active,[41] consistent with the assumption that the coordination itself comprises the limiting factor. Indeed, extensive solid state NMR relaxation studies are currently under way to verify this presumption and in order to obtain more details on the ion dynamics. In addition, transference number studies of the blends will provide important information on the dominant contribution to the observable conductivity.

CONCLUSIONS

In the present work, well-defined model compounds based on CTP and HPB cores with tethered Li^+-solvents were successfully synthesized. Adequate CTPs were obtained upon reaction of $N_3P_3Cl_6$ with appropriate alkenoles, followed by epoxidation with MCPBA and catalytic CO_2 insertion. In the epoxidation step, *equimolar* amounts of antioxidant BHT are essential to prevent degradation of the CTP cycle.

The synthesis of the HPB-based model compounds starts by reacting hexakis-(4-hydroxyphenyl)-benzene with an enoyl chloride. The buildup of the 2-oxo-1,3-dioxolane side group follows the description for the CTP model substances; however, for the catalyzed CO_2 insertion, a high CO_2 partial pressure of about 80 bar was significant to obtain full conversion.

The well-defined model compounds show the onset of decomposition above 250 °C and cover a broad range of glass transition temperatures from −79 °C for the oligo(oxyethylene) functionalized CTP up to +3.5 °C for the HPB-based model compound featured by an alkyl chain of eight carbons between a core and Li^+-solvating group.

All considered model compounds represent good solvents for LiTFSI. Notably, for the CTP-based compounds even, no significant differences in ionic conductivity were observed for the blends with various lithium salts including LiBETI, LiBOB, or $LiClO_4$. In addition, the temperature-dependent ionic conductivities of the blends follow a William−Landel−Ferry (WLF) type behavior with the corresponding glass transition temperatures as the reference temperature. The highest obtained conductivity value was 6.0×10^{-6} at 40 °C for the CTP model bearing the longest alkyl spacer of eight carbons between the core and solvating group, while shorter alkyl spacers reveal reduced ionic conductivities. The HPB models exhibit higher glass transition temperatures and conductivities at 40 °C being about 2 orders of magnitude lower than their CTP analogues. However, compared to the previously studied poly(meth)acrylate analogues with much higher glass transitions,[12] especially the conductivity of the low-T_g CTP models was unexpectedly low. The discrepancy between low glass transition temperatures and rather low ionic conductivities most likely indicates too strong interactions between lithium ions and the solvating 2-oxo-1,3-dioxolane moieties. This may hinder fast lithium ion mobility, thereby causing lower ionic conductivities. Following the Pearson concept, *softer* solvating moieties should be taken into account for future studies. Furthermore, in order to prove the discussed statements and to obtain more detailed information on the system dynamics, extended solid state NMR relaxation studies are currently in progress as well as transference number measurements.

AUTHOR INFORMATION

Corresponding Author

*E-mail: meyer@mpip-mainz.mpg.de. Tel.: +49 (0)6131 379 400. Fax: +49 (0)6131 379 480.

ACKNOWLEDGMENT

The authors gratefully acknowledge assistance in the synthetic work by A. Manhart and in retrieving impedance spectroscopy data by C. Sieber. P. Räder is acknowledged for assistance in obtaining thermal analytical data of the model compounds as is M. Wagner for supporting the ^{31}P NMR spectroscopy. This research was supported by the *International Max Planck Research School*.

REFERENCES

(1) Winter, M.; Brodd, R. J. *Chem. Rev.* **2004**, *104*, 4245.
(2) Scrosati, B. *JEC Battery Newsletters* **1993**, *6*, 44.
(3) Schalkwijk, van, W., Scrosati, B., Eds. *Advances in Lithium-Ion Batteries*; Kluwer Academic/Plenum: New York, 2002.
(4) Zhang, S. S. *J. Power Sources* **2007**, *164*, 351.
(5) Xu, K. *Chem. Rev.* **2004**, *104*, 4303.
(6) Tsutsumi, H.; et al. *Solid State Ionics* **2003**, *160*, 131.
(7) Vogdanis, L.; Martens, B.; Uchtmann, H.; Hensel, F.; Heitz, W. *Macromolekul. Chem.* **1990**, *191*, 465.
(8) Fenton, D. E.; Parker, J. M.; Wright, P. V. *Polymer* **1973**, *14*, 589.
(9) Meyer, W. H. *Adv. Mater.* **1998**, *10*, 439.
(10) Lewandowski, A.; Swiderska-Mocek, A. *J. Power Sources* **2009**, *194*, 601.
(11) Stephan, A. M.; Nahm, K. S. *Polymer* **2006**, *47*, 5952.
(12) Britz, J.; Meyer, W. H.; Wegner, G. *Macromolecules* **2007**, *40*, 7558.
(13) Lauter, U.; Meyer, W. H.; Wegner, G. *Macromolecules* **1997**, *33*, 2092.
(14) Allcock, H. R. *Chemistry and Applications of Polyphosphazenes*; Wiley-Interscience: New York, 2003; p 528.
(15) Kaskhedikar, N.; Burjanadze, M.; Karatas, Y.; Wiemhöfer, H. D. *Solid State Ionics* **2006**, *177*, 3129.
(16) Tada., Y.; Sato, M.; Takeno, N. *Macromol. Chem. Phys.* **1994**, *195*, 1923.
(17) Andrianov, A. K.; Marin, A.; Peterson, P. *Macromolecules* **2005**, *38*, 7972.
(18) DeCollibus, D. P.; Marin, A.; Andrianov, A. K. *Biomacromolecules* **2010**, *11*, 2033.
(19) Jimenez-Garcia, L.; Kaltbeitzel, A.; Pisula, W.; Gutmann, J. S.; Klapper., M.; Muellen, K. *Angew. Chem., Int. Ed.* **2009**, *48*, 9951.
(20) Sugimoto, H.; Kuroda, K. *Macromolecules* **2008**, *41*, 312.
(21) Sakurai, T.; Yamamoto, K.; Naito, H.; Nakamoto, N. *Bull. Chem. Soc. Jpn.* **1976**, *49*, 3042.
(22) Paddock, R. L.; Hiyama, Y.; McKay, J. M.; Nguyen, S. T. *Tetrahedron Lett.* **2004**, *45*, 2023.
(23) Allcock, H. R.; Ravikiran, R.; O'Connor, S. J. M. *Macromolecules* **1997**, *30*, 3184.
(24) Gaul, C.; Njardarson, J. T.; Shan, D.; Dorn, D. C.; Wu, K.; Tong, W. P.; Huang, X.-Y.; Moore, M. A. S.; Danishefsky, S. J. *J. Am. Chem. Soc.* **2004**, *126*, 11326.
(25) Kobayashi, K.; Shirasaka, T.; Sato, A.; Horn, E.; Furukawa, N. *Angew. Chem., Int. Ed.* **1999**, *38*, 3483.
(26) Lu, Y.; Suzuki, T.; Zhang, W.; Moore, J. S.; Marinas, B. J. *Chem. Mater.* **2007**, *19*, 3194.
(27) Buizide, A.; LeBerre, N.; Sauve, G. *Tetrahedron Lett.* **2001**, *42*, 8781.
(28) Tohda, Y.; Sonogashira, K.; Hagihara, N. *J. C. S. Chem. Commun.* **1975**, *2*, 54.
(29) Fantin, G.; Medici, A.; Fogagnolo, M.; Pedrini, P.; Gleria, M. *Eur. Polym. J.* **1993**, *29*, 1571.
(30) Baba, A.; Nozaki, T.; Matsuda, H. *Bull. Chem. Soc. Jpn.* **1987**, *60*, 1552.
(31) Ochiai, B.; Hatano, Y.; Endo, T. *J. Polym. Chem. Part A* **2009**, *47*, 3170.
(32) Movassaghi, M.; Jacobsen, E. N. *J. Am. Chem. Soc.* **2002**, *124*, 2456.
(33) Bonsignore, S.; Dalcanale, E.; Martinengo, T. *Synth. Commun.* **1988**, *18*, 2241.
(34) Regla, I.; Luviano-Jardón, A.; Demare, P.; Hong, E.; Torres-Gavilán, A.; López-Munguía, A.; Castillo, E. *Tetrahedron: Asymm.* **2008**, *19*, 2439.
(35) Doughty, S. W.; Fitzsimmons, B. W.; Reynolds, C. A. *J. Chem. Soc., Dalton Trans.* **1997**, 367.
(36) Williams, M. L.; Landel, R. F.; Ferry, J. D. *J. Am. Chem. Soc.* **1955**, *77*, 3701.
(37) Armand, M.; Gorecki, W.; Andreani, R.; Scrosati, B. *Second International Symposium on Polymer Electrolytes*; Elsevier Applied Science: New York, 1989; p 91.
(38) Ratner, M. A. *Polymer Electrolyte Reviews*; MacCallum, J. R., Vincent, C. A., Eds.; Elsevier: London/New York, 1987; Chapter 7.
(39) Zhang, Z.; Lyons, L. J.; Jin, J. J.; Amine, K.; West, R. *Chem. Mater.* **2005**, *17*, 5646.
(40) Zhang, Z.; Lyons, L. J.; West, R.; Amine, K.; West, R. *Silicon Chem.* **2005**, *3*, 259.
(41) McCrum, N. G.; Read, B. E.; Williams, G. In *Anelastic and Dielectric Effects in Polymeric Solids*; Wiley-Interscience: New York, 1967; Chapter 8, p 238.